CORE
Metadata, citation and similar papers at core.ac.uk
Provided by Elsevier - Publisher Connector

Archives of Biochemistry and Biophysics 602 (2016) 21–31

Contents lists available at ScienceDirect

Archives of Biochemistry and Biophysics

journal homepage: www.elsevier.com/locate/yabbi

Current advances in synchrotron radiation instrumentation for MX experiments☆

Robin L. Owen [a], Jordi Juanhuix [b, *], Martin Fuchs [c]

[a] Diamond Light Source, Harwell Science and Innovation Campus, Didcot, OX11 0DE, UK
[b] Alba Synchrotron, Carrer de la llum 2-26, Cerdanyola, 08192, Spain
[c] National Synchrotron Light Source II, Brookhaven National Lab, Upton, NY, 11973, USA

ARTICLE INFO

Article history:
Received 17 December 2015
Received in revised form
16 March 2016
Accepted 21 March 2016
Available online 1 April 2016

Keywords:
Macromolecular crystallography
Synchrotron radiation
Beamline instrumentation
X-ray diffraction
Review
Experimental methods

ABSTRACT

Following pioneering work 40 years ago, synchrotron beamlines dedicated to macromolecular crystallography (MX) have improved in almost every aspect as instrumentation has evolved. Beam sizes and crystal dimensions are now on the single micron scale while data can be collected from proteins with molecular weights over 10 MDa and from crystals with unit cell dimensions over 1000 Å. Furthermore it is possible to collect a complete data set in seconds, and obtain the resulting structure in minutes. The impact of MX synchrotron beamlines and their evolution is reflected in their scientific output, and MX is now the method of choice for a variety of aims from ligand binding to structure determination of membrane proteins, viruses and ribosomes, resulting in a much deeper understanding of the machinery of life. A main driving force of beamline evolution have been advances in almost every aspect of the instrumentation comprising a synchrotron beamline. In this review we aim to provide an overview of the current status of instrumentation at modern MX experiments. The most critical optical components are discussed, as are aspects of endstation design, sample delivery, visualisation and positioning, the sample environment, beam shaping, detectors and data acquisition and processing.
© 2016 Diamond Light Source Ltd. Published by Elsevier Inc. This is an open access article under the CC BY license (http://creativecommons.org/licenses/by/4.0/).

1. Introduction

The first successful proof-of-principle of macromolecular crystallography (MX) experiments at synchrotron accelerators were performed in the mid 1970s [124] [67,117]. These structures have allowed the visualisation of proteins and viruses on an atomic level, and led to a much greater understanding of the function of the building blocks of life. The relevance of this knowledge has been recognized through the award of a large number of Nobel prizes (summarised in Ref. [21]) Over these 40–50 years, synchrotron sources, beamlines and experimental approaches have constantly evolved, dramatically changing what is considered possible, or can be obtained, from an MX experiment. Recent reviews, such as those by Refs. [38,46] give an excellent overview of the history of MX and synchrotron radiation.

As an illustration of the impact of synchrotron radiation on MX and the rate at which the field is expanding, the number of structures held in the Protein Data Bank (PDB) at the time of these reviews and now can be compared. In 2010, the PDB comprised ~60,000 structures of which ~73% were determined at a synchrotron. At the time of writing, the number of structures has increased to more than 112,000 with synchrotrons now accounting for ~77% of the total number of depositions and approximately 90% of all new depositions. This rate of increase is reflected in challenging sub-areas of the field such as membrane protein crystallography where the number of unique structures has increased from 280 to 518 over the last five years. The striking increase in both the number and rate of depositions is, in no small part, due to continuing advances in beamline instrumentation, experimental approaches and tools to facilitate MX at X-ray sources.

There are now over 100 beamlines dedicated to MX at more than 20 synchrotrons worldwide[1] (Fig. 1) and the instrumentation in all areas of these beamlines has continued to evolve. This evolution has driven scientific discoveries, much in the way put by

☆ This article is part of a Special Issue entitled Protein Crystallography, edited by Ana Camara-Artigas and Jose Antonio Gavira

* Corresponding author.
E-mail addresses: robin.owen@diamond.ac.uk (R.L. Owen), juanhuix@cells.es (J. Juanhuix), mfuchs@bnl.gov (M. Fuchs).

[1] http://biosync.sbkb.org.

http://dx.doi.org/10.1016/j.abb.2016.03.021
0003-9861/© 2016 Diamond Light Source Ltd. Published by Elsevier Inc. This is an open access article under the CC BY license (http://creativecommons.org/licenses/by/4.0/).

Fig. 1. Current worldwide distribution of MX beamlines. Area of the outer circle is proportional to the number of MX beamlines currently operating at the facility.

Sydney Brenner in 1980 – "Progress in science depends on new techniques, new discoveries, and new ideas, probably in that order" [122]. Crystals of poor diffraction quality that previously would have required spending another year in the crystallization lab for optimization, can now provide complete datasets and lead to successful structure determination. Generally, beamline scientists attempt to set up their data acquisition interface with default settings to maximize the data quality users can obtain. However, it is often successful communication between the structural biologist, to describe the challenges of the sample, and the beamline scientist, to describe new advances in instrumentation and software, that really makes the difference in meeting experimental goals. New techniques or instrumentation often originate from pioneering experiments or developments at 'standard' MX beamlines. The success of the technology developed for MX beamlines also inspires other synchrotron fields such as powder diffraction and small angle scattering, which are adopting instruments such as the robotic sample manipulators or the experiment control software.

This review therefore, while attempting to touch on historical developments, focuses on outlining the current state of the art of MX beamline instrumentation, and tries to point out the ongoing and new trends and developments such as an increasing degree of automation, increasing numbers of experiments performed with remote access, cross fertilization with free electron laser experiments, micro- and nano-crystallography, native SAD phasing, in-situ room temperature data collection and multi-crystal and serial crystallography.

2. X-ray source, optics and diagnostics

2.1. X-ray sources

The first "parasitic" protein crystallography data collections, at synchrotron accelerators primarily dedicated to high-energy physics, exposed the potential of purpose-built facilities for the field of MX [67,117,124]. The first dedicated synchrotron sources (DORIS, Hamburg-Germany; SRS, Daresbury-UK; NSLS, Brookhaven-USA; Photon Factory, Tsukuba-Japan) started operation in the early 1980s with bending magnet beamlines dedicated to MX. Synchrotron sources made another step forward in the 1990s with the advent of 3rd generation sources which featured a lower emittance and the extended use of insertion devices (ID) installed in straight sections as a photon source for beamlines. The photon flux, beam size and beam divergence of these photon sources match the weak diffracting power, small crystal size, and the large unit cell parameters of typical macromolecular crystals.

Insertion devices (IDs) are periodic arrays of magnets which bend the path of the electrons as they circulate the storage ring. Changes in the electron beam trajectory at each magnet results in the emission of radiation. Undulators are IDs that exploit constructive interference between the radiation emitted at different periods and are the brightest photon source at current synchrotrons [3]. This constructive interference results in sharp peaks in the spectral profile where the intensity of radiation produced is proportional to the square of the number of poles. Undulators can emit radiation at the wavelengths typically used in MX (around 1 Å) only in storage rings with electron energy above ~2.25 GeV. Below this energy, radiation of around 1 Å must be emitted by wigglers, where the interference is no longer preserved and the flux is proportional to the number of poles: a significant reduction.

New developments to greatly reduce the emittance and increase the brilliance of storage rings, and hence improve the X-ray beam properties achievable at the sample position, are now being realised [69,147]. By using damping wigglers and increasing the circumference, the NSLS-II currently achieves the smallest sub-nm rad horizontal emittance in regular operation [149]. In a new fourth generation of storage rings, the multibend achromat magnetic lattices [48,49] allow the construction of diffraction-limited storage rings [10], typically of circumference 500–1500 m and possessing an emittance below 0.4 nm rad. The first fourth generation storage ring due to become operational is MAX IV in Lund, Sweden, which will begin operation in 2016 [138]. Such is the attraction of these storage rings that several other such sources are under construction, and the lattice of a number of existing sources is being redesigned. The X-ray beams produced by these new sources will represent an increase by a factor of 20 in brilliance and ~1.5 in flux in comparison to third generation sources.

Aided by the smaller emittance of the new storage rings, a new generation of undulators using superconducting magnets [58] or,

especially, cryogenic permanent magnets [66] aims at reducing the magnetic period. A shorter undulator period is of interest, as it allows for a reduction of the electron energy required for the generation of a specific photon wavelength, a larger number of periods per length (resulting in higher flux), an increased spectral tunability, and an increase of the radiation hardness of the undulator.

2.2. Monochromators

The beamline monochromator selects X-rays of a single wavelength from the broad energy spectrum emitted by the bending magnet or insertion device, and also absorbs the power of the disregarded energies. A historical overview of the development of monochromators at synchrotron sources is given by Ref. [12]. Briefly, the photon wavelength is selected using Bragg's law and can be varied by changing the angle of crystals with respect to the incoming beam. The means of crystal mounting is chosen according to the design priorities of the beamline. Currently the most popular type of monochromator is the double-crystal monochromator (DCM), in which the second crystal surface is adjusted to maintain a fixed beam path after the monochromator at any photon wavelength. By sagittally bending one of the monochromator crystals, the x-ray beam can be focused horizontally. Also, two identical DCMs placed oppositely can be used to maintain the beam path after the monochromator at any selected wavelength [8]. An alternative to a DCM is the channel-cut monochromator (CCM), in which the two crystal surfaces are part of the same silicon block. CCMs are less prone to introduce beam vibrations and drifts, but change the path of the output beam when the beamline energy is changed, unless two identical channel-cut crystals are used as in the case of the Bartels monochromator. For long microfocus beamlines, the required high stability of the monochromator crystals can indicate a design with a vertical rotation axis [57], which minimizes the projection of gravity onto the Bragg axis and greatly reduces the construction's height above the supporting granite structure. Moreover, since the source size is still larger in the horizontal than in the vertical direction, a horizontal diffraction plane has less influence on the beam stability. Due to its axis being perpendicular to the x-ray polarization, this sacrifices some flux at long wavelengths and energy resolution for a more stable construction.

Silicon crystals are very well suited for selecting the photon wavelength for MX experiments and high quality crystals can be obtained at relatively modest cost. Moreover, silicon has excellent physical properties at cryogenic temperatures: the coefficient of thermal expansion at liquid nitrogen temperatures is close to zero and the thermal conductivity is largely increased with respect to room temperature. Monochromator silicon crystals are usually cut such that the crystal surface is parallel to a Bragg plane (symmetric cut), for ease of manufacturing and to preserve both beam size and divergence when changing the photon energy.

The most commonly used silicon reflection is (111) as it delivers a strong diffracted beam due to its large structure factor. Moreover, the natural width of the (111) reflection is similar to the typical vertical photon beam divergence. This similarity maximizes the flux while keeping an energy bandpass of $\Delta E/E \sim 2 \cdot 10^{-4}$ low enough to allow energy-dependent experiments. Other advantages of silicon are that the lattice parameter ($d = 3.1356$ Å) allows a large deflection angle of $2\theta \sim 18.5$ deg at a wavelength of 1 Å, and the diamond cubic symmetry of the crystal structure results in the absence of a (222) reflection and thus the possible presence of X-rays of twice the desired energy at the sample position. Other reflections, notably (220) and (311), have been used to improve the energy resolution at the expense of a lower photon flux at the sample. Nonetheless the use of these reflections is limited as only a small subset of experiments greatly benefit from this increased energy resolution. Multilayer monochromators with a wide energy bandpass, and hence large photon flux throughput, are currently being developed and installed in order to exploit high frame rate detectors and new fast data collection strategies.

2.3. Focusing optics

The role of beamline optics is to focus the cone of X-rays emitted by the photon source to a size comparable to, or smaller than, the sample. Concurrently, the beam divergence, which increases by the same factor as the size is reduced, must be minimised to avoid increasing the apparent crystal mosaicity seen on the diffraction pattern. The variety of source properties, and scientific cases at MX beamlines has led to a number of optical layouts. Some representative examples are shown in Fig. 2.

Curved reflective mirrors with lengths between 0.2 and 1 m are the most common method for focusing the X-ray beam onto the sample or the detector position, or to create a secondary source in a 2-step focusing scheme. Aberration-free focussing can be achieved through use of an ellipsoidal surface although toroidal and spherical shapes are used as well. Mirrors made of silicon, fused silica or ceramic and coated with one or several high-Z metal stripes (usually Rh, Pd, Pt, Ir) are placed at typical grazing incidence angles of ~0.3 deg to ensure total external reflection. As reflectivity of these coatings falls dramatically above an element-dependent cut-off energy, the mirror effectively removes any higher harmonics passing the monochromator.

One of the mirror configurations most commonly used is the Kirkpatrick-Baez (KB) arrangement, consisting of a pair of plane-elliptical mirrors mounted orthogonally, so that the beam can be adjusted independently in horizontal and vertical dimensions. Meridional optics (curved along the beam direction) such as these have a long radius of curvature (0.2–10 km) and this is often achieved by bending a plane surface or through use of bimorph mirrors [154], in which a piezo-actuator is attached every ~20 mm along the length of the mirror. Adaptive mirror optics based on mechanical actuators are also under study.

Very strict tolerances on the mirror slope errors are required to maintain the source brightness in low-emittance synchrotrons and Free Electron Lasers (FELs). Roughness of the mirrors has the effect of broadening the spot size, while longer period slope errors are additionally the major source of beam heterogeneities, especially when the beam is defocused to match the crystal dimensions. Several approaches have been used to improve the surface quality in mirrors. Classical mechanical polishing using massive planetary polishing systems is proven to achieve flat mirror surfaces to 0.2 μrad RMS. New innovative approaches are Ion Beam Figuring [155] and, in particular, Elastic Emission Machining (EEM) [156]. The EEM technique, offered by J-Tec (Osaka, Japan), can achieve a RMS slope error of less than 50 nrad and a figure accuracy of <1 nm in a 350 mm-long mirror and is the current state-of-the-art. Advances on mirror polishing have been only possible with accompanying new optical metrology instruments, notably the Nanometer Optical Metrology ('NOM') long-trace linear profilometers [157]. Monitoring of the surface quality is possible with in-situ, at-wavelength methods such as the pencil beam method or the shearing interferometry [148]. Overall, these advances have led to a 5-fold improvement of the mirror surface quality in the last 10 years.

An alternative to reflective optics are refractive lenses which exploit the slightly different refractive index between light-Z materials (Be, Al, Si) and vacuum to focus the X-ray beam [158]. Transfocators are arrays of refractive lenses that can focus the beam

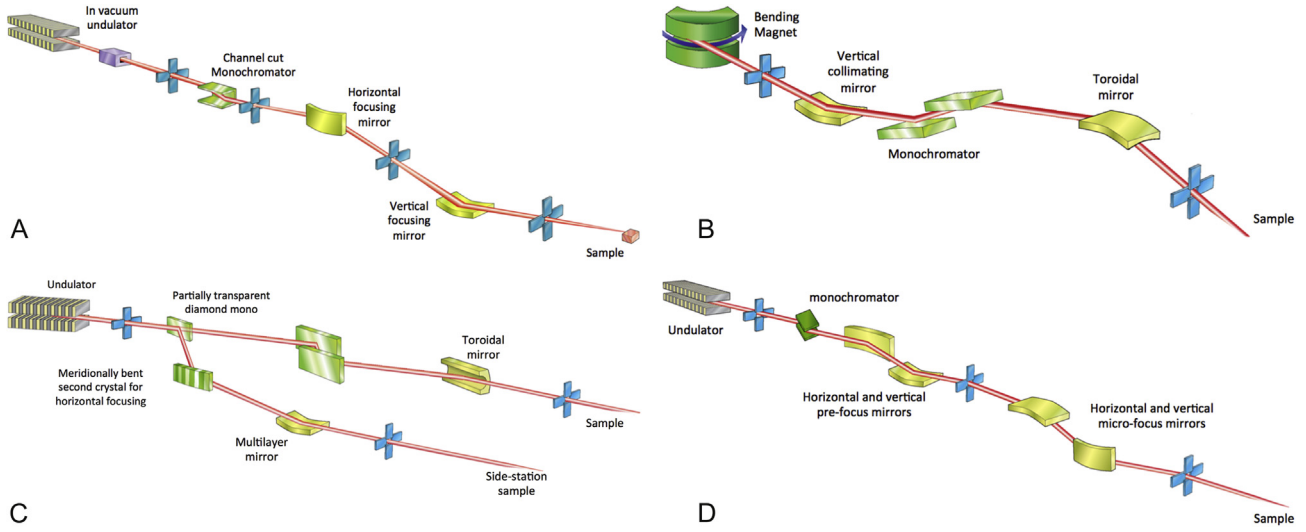

Fig. 2. Schematics of different optical arrangements used at MX beamlines. In an effort to include a variety of optical elements some schemes incorporate aspects of multiple beamlines, and so may not represent an actual beamline. A. Undulator beamline with a double crystal monochromator and focusing provided by two mirrors in a KB arrangement. B. Bending magnet beamline showing the X-ray beam collimated in the vertical by a collimating mirror placed before the double crystal monochromator. C. Undulator beamline with a fixed-wavelength sidestation. A fraction of the beam from the undulator is deflected by a partially transparent monochromator crystal. The beam passing through is incident on a double crystal monochromator and then focused using a toroidal mirror. D. Two-stage focusing arrangement for obtaining a micro-focused beam at the sample position.

in one or two dimensions depending on the lens shape [141]. The photon energy and the number of identical lenses brought to the beam path determine the focusing distance. Although transfocators deliver less flux due to the limited transmission through the lenses, the beam is very stable and the change of the beam size (i.e. the focus) or the energy which imply changing the number of lenses, take only a few minutes. The use of transfocators is currently expanding worldwide, especially in Europe, being particularly interesting for beamlines offering small beam sizes and moderate to high photon energies, or concerned to reduce the wavefront distortions.

With the improvement of the source and focusing technologies, there are now over 20 microfocus beamlines worldwide with beam sizes below 20 μm [133] with beamlines under construction to achieve beam sizes even below 1 μm.

2.4. Diagnostics

To maximize the signal-to-noise and overall data quality of macromolecular crystallography data sets, the size and divergence of the X-ray beam should be matched to the crystal properties [34,107]. It is the beamline diagnostics system that provides feedback on the current value and stability over time of these beam parameters.

Beyond interactive beam optimization, beam diagnostics are critical for automatic beamline operation, and for the logging of experiment parameters to image headers or other metadata information to inform data processing. Beam diagnostic information is essential for data collection strategy planning. With the beam profile available, the 3D dose distribution within a crystal can be visualised and integrated in the experiment planning by RADDOSE-3D [152]. Last but not least, diagnostics are a means for the user's verification of the beamline's proper operation – is a lack of diffraction due to the sample or is it the beamline?

Beam monitors can provide intensity, position, and shape or profile information, with different types providing different combinations of these three key parameters. The main performance specifications of beam monitors are beam transmission, sensitivity, radiation hardness, time resolution, dynamic range, size, and photon energy dependence. Invasive monitors such as fluorescent screens that completely block the beam are often used for commissioning the beamline. Diagnostics in use during data collection have to be transmissive, such as the monitor types discussed below.

In addition to controlling the beam parameters, ensuring the beam's stability [120] is crucial for optimising data quality. In case it is impossible or impractical to identify and remove them, beam-drifts, and to some extent also vibrations, can be stabilized through position feedback schemes. Typically, the measured beam position is used as a corrective input to beam steering optical elements such as X-ray mirrors or monochromator crystals. The speed of such feedback systems depends on the mechanical properties of the optical elements, which place a practical limit around 10 Hz. Beam stabilization can also be achieved by steering the electron beam orbit via the storage ring magnets [26], also at higher frequencies [106]. Moreover, feedback on monochromator crystal angular settings can be used to stabilize the X-ray beam energy and intensity [15,85,140], and in principle the stabilization of the full beam profile is possible.

Monitors for white beams require special solutions that can handle the high heat load. Blade beam position monitors measure photo currents from tungsten or diamond blades exposed to the X-ray beam fringes [14,73,76,132]. Quadrant electrode monitors obtain photocurrents from a thin diamond membrane [103]. For both monitor types, a position is derived from the differential signal coming from the sensors located in opposite sides of the beam.

For monochromatic X-ray beams, a variety of position monitors are used: CVD diamond quadrant electrode photo current monitors with a polycrystalline [130,131], (Dectris Rigi) or a single crystalline membrane [42,92,103], quadrant diode monitors detecting back-scatter fluorescence from a metal foil [2] and split electrode ion chambers [97,128,129]. All of these can double as intensity monitors. An intensity monitor combined with an aperture that cuts into the beam can also provide dynamic positional information such as the frequency spectrum of vibrations, or – given the beam profile – relative position data.

Pixelated CVD diamond quadrant electrode monitors can provide beam profile data [153]. The NanoBPM profile monitor [81]

commercialised by FMB Oxford is essentially a pinhole camera observing the fluorescence generated by the X-ray beam footprint in a thin membrane.

3. Endstation and experiment

3.1. Endstation

In designing a macromolecular crystallography beamline's experimental station, several partially opposing requirements have to be considered: Performance, versatility, flexibility, ease of use, size, and automated operation. These conflicting requirements together with other constraints such as source and optical parameters, and even the available space and resources, mean that many different approaches have been adopted to design the core functionality of an MX endstation. Typically this functionality encompasses sample movement and positioning, sample visualisation, temperature control, and automated sample exchange.

Several key boundary conditions have greatly evolved throughout the years, thereby greatly changing the requirements for experimental stations. Beam sizes and average sample sizes shrunk from millimetres to a few microns and data collection times have diminished from days to minutes and now seconds due to the development of faster detectors and brighter X-ray beams. To follow these advances, endstation designers had to improve goniometer precision, microscope resolution, incorporate sample automation, and greatly improve the overall stability of the apparatus.

An example of a highly integrated, high-precision and widely implemented design for an experimental station is the EMBL/ESRF MD2 microdiffractometer [114] and its successor, the MD3, both of which have been commercialised.[2] At the other extreme, the use of a six axis robotic arm as a basis for a diffractometer in the G-Rob [87] or the ESRF RoboDiff [102] is an implementation designed for highest possible flexibility and throughput. An example for extreme versatility in terms of the experiments possible at a single beamline is the PETRA III P11 beamline combining macromolecular crystallography, imaging, and time-resolved techniques into one single experimental station for bio-imaging and diffraction [96]. Endstation layouts at MX beamlines worldwide have been developed to make optimal use of the locally available spatial conditions, such as so-called mini-hutches that provide user-access to the sample area through a small window, rather than requiring the opening of the hutch-door [90]. Several experimental stations have added specialized features, such as advanced visualisation techniques like fluorescence imaging [63] or SONICC detection [91], or concurrent optical spectroscopies and data collection from crystallization plates (both discussed below). Beamlines that aim to provide extreme figures of merit require dedicated solutions, such as the optimization for smallest beam and crystal sizes for micro- and nano-crystallography [121], or for longest wavelengths with helium-flooded [71] or even in-vacuum sample environments [105].

The experimental stations at the authors' beamlines may serve as illustrative examples of the variation of designs laid out above (see Fig. 3). The experimental station of the XALOC beamline at the ALBA synchrotron has at its core the microdiffractometer MD2 [80]. The D3 diffractometer at the Swiss Light Source [56] combines a microcrystallography goniometer with an in-situ on-axis microspectrophotometer for concurrent UV/Vis absorption, fluorescence and Raman spectroscopy. The I24 endstation at Diamond provides two separate goniometers for rapidly switching between microcryocrystallography and high precision room-temperature crystallography in plates (initial design overview given in Ref. [65]).

3.2. Sample positioning

The goniometer is central in the oscillation crystallographic method used in almost every MX experiment, in which the crystal rotates while recording diffraction images. Goniometer technology has seen an evolution from the use of mechanical bearings to air bearings, and from the use of large circles carrying proportional detectors to small goniometer spindles rotating the crystal while the diffraction pattern is recorded simultaneously with an area detector. Arguably the key performance parameter of a goniometer is its sphere of confusion – the smallest sphere containing the goniometer's sample mount position while rotating through its complete parameter space. The requirements on a goniometer's sphere of confusion are dictated by the size of crystals measured, the size of the beam, and the Bragg angle range over which crystals are rotated during a data collection. Assuming the experimenter has carefully matched the beam size to the crystal size, and wants to collect a 180° wedge, the sphere of confusion should typically be less than 10% of the beam and crystal size. Reductions in both of these parameters to the single micron scale have driven forward goniometer technology.

Modern microcrystal diffractometers have been able to achieve sub-micron spheres of confusion (see for example the D3 diffractometer [56], the Kohzu QKSU-1 goniometer [71] and the MD3 microdiffractometer, though many others now exist at, for example, beamlines such as I24 at Diamond, GM/CA at APS, and P11 at PETRA III). By measuring the reproducible error of a goniometer, the angular dependence of a goniometer's gravitational sag can be determined and stored in a lookup table, to be used in as part of an active correction scheme to reduce the goniometer's sphere of confusion. With their rotational axis aligned to the gravitational force, vertical axis goniometers typically can achieve smaller spheres of confusion of around or even below 100 nm [84,121]. In principle, for longer wavelengths the horizontal polarization of the synchrotron radiation may limit the diffraction resolution attained by vertical axes in the oscillation method for crystallographic data collection as used in MX [4]. Nevertheless, to the authors' best knowledge, for the resolutions and data qualities typical in MX, current experiments are yet to encounter this limitation.

Multi-axis goniometers, providing three rotational degrees of freedom, open the possibility for further optimization of data collection strategies [20]. These strategies include the reorientation such that Friedel pairs are recorded on the same image to aid anomalous phasing, or the alignment of the crystal with a long crystal axis along the rotation axis to minimise diffraction spot overlap. The orientation of the unit cell axes is typically determined via software such as XOalign[3] following collection of a small number of indexing frames.

Due to geometrical constraints and their comparatively large sphere of confusion, multi-axis goniometry has not been extensively used in the past decade. However, such goniometry mounted on the omega axis has met increasing interest: first with the minikappa device in combination with the MD2 and MD3 diffractometers [20] and more recently with the PRIGo [145].

While the classical oscillation method consisted of centering a crystal in the beam and then rotating it while recording diffraction images, the use of line, or helical, scanning [159] has become an increasingly common means of collecting crystallographic data. By

[2] http://www.arinax.com.

[3] https://code.google.com/p/xdsme/.

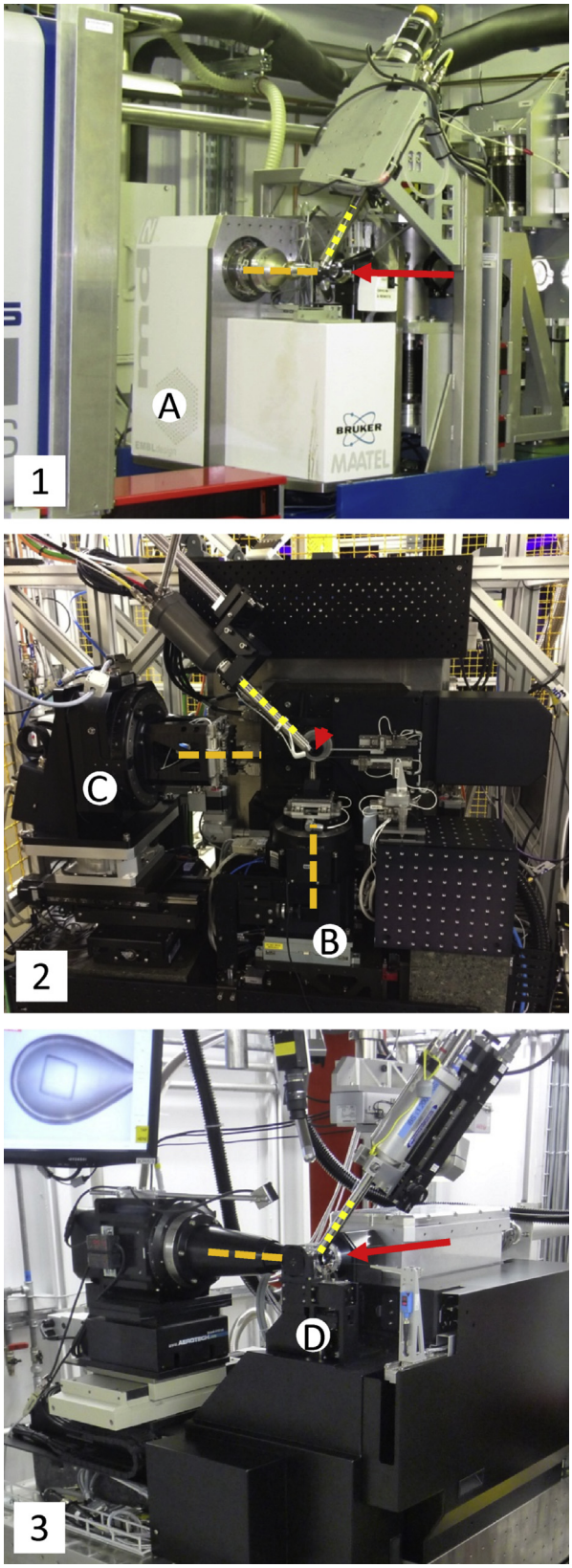

Fig. 3. Experimental stations (ES) of the beamlines XALOC at ALBA (1), I24 at Diamond Light Source (2) and X10SA at the Swiss Light Source (3). The beam direction is indicated by the red arrow, goniometer spindles by the orange dashed lines and the cryo cooler nozzle by the yellow dotted lines. The XALOC ES is built around the micro-diffractometer MD2 (Arinax, France) (A). The I24 ES features two goniometers, the main goniometer with a vertical spindle (B) and a dedicated crystallization plate goniometer with a horizontal spindle (C). The X10SA diffractometer D3 features a microspectrophotometer for concurrent diffraction and optical spectroscopy experiments (D).

translating a crystal in a synchronized movement with the omega rotation, a helical path through/along a crystal is traced. Translation during exposure to X-rays means that the absorbed dose can be evenly distributed over the crystal, to make optimal use of the diffracting volume and avoid discontinuities in the scaling correction that would result from collecting data from discrete positions. In addition to the beam trajectory, an optimal data collection strategy has to include a suitable beam shape – for a needle-shaped crystal, this could be a vertical line focus swept along the needle – and the distribution of the X-ray dose, see below.

3.3. Beam shaping and sample environment

Optimization of data collection includes careful tailoring of the X-ray beam properties to the crystal. By adjusting the beam focus to the size of the crystal, the background scattering from the buffer surrounding the crystal can be minimized and signal to noise maximised [51]. Where the beamline's native focus is larger than the sample, the beam size can be adjusted at the expense of flux through the use of slits or pinhole apertures (as demonstrated for example at GM/CA, APS [53] or offered as part of the functionality of the MD2 microdiffractometer). For crystal morphologies such as plates, for optimal data collection the beam shape should be changed as the crystal rotates such that the beamsize matches the projected dimensions of the crystal along the beam axis [68] – while this ideal approach is not commonly implemented yet, a beamsize adjustment to the average projection size is good common practice. Alternatively, the beam is sometimes expanded at the sample position by defocusing the mirrors to uniformly illuminate the crystal or to focus the beam at the detector.

For all experiments, care must be taken to minimise the contribution of air scatter to the data collected. Most frequently this is addressed through the use of a collimating tube that encloses the beam to within a few mm of the sample. For micro-crystal data collection, and data collection at long wavelengths, absorption and scattering by air becomes a significant limitation and additional care is required. Air scatter can be reduced through the use of a helium path between the beam stop and detector surface, switching the sample cooling from gaseous nitrogen to helium, or even by encasing the complete endstation environment and flushing it with He gas [71]. Further gains – especially crucial for measurements at long wavelengths – can be made through use of an in vacuum endstation as, for example, at beamline I23 at Diamond Light Source [105].

Sample cooling using a nitrogen gas flow at cryogenic temperature is an essential part of all ‘standard’ MX experiments at synchrotron sources (radiation damage aspects of cryo-cooling are discussed below). Further control of the sample cooling can be achieved through the use of a cryo-shutter that allows controlled sample annealing. Under certain circumstances, this can improve the diffraction quality of a crystal, though the chances of success can be hard to predict. For room temperature measurements, the use of humidity control devices [127] can prevent samples from drying out. By monitoring the diffraction properties of the crystal as humidity conditions vary, improvements in crystal quality can be found in some cases [18]. A key consideration in the endstation design is temperature stability: the effects of cold nitrogen gas can be mitigated through the use of a cryo gas extraction tube opposite the cryo nozzle, which will also reduce the nitrogen flow turbulence. The use of on-axis cryo-cooling, with a heating shield

between the sample pin and goniometer to stabilize its temperature, greatly reduces the sample pin's projection to the gas flow [11]. Automation also helps improve temperature stability as the need to open the experimental hutch regularly is removed.

Data collection from crystals held in crystallographic plates, or *in situ* data collection, is routinely used for both crystal screening and the collection of datasets. As crystallization trays were not initially designed with X-ray data collection in mind, an early use case was to obtain rapid feedback on the crystal identity and on the quality of hits in crystallization trials. As the data collected at room temperature is free of artefacts from handling, cryo-protectants and from the cooling process itself, *in situ* data collection can provide a rapid means of optimising crystallization conditions. The first implementations used a six-axis robotic arm with a gripper for SBS format crystallization plates to position and rotate the plates in the X-ray beam [77], while more recent implementations have incorporated dedicated goniometry into the endstation [7,13,87]. Crystallization plates have also evolved to facilitate X-ray data collection, with plates designed to minimise background scatter and maximize the accessible rotation range becoming commercially available. *In situ* plates compatible with lipidic cubic phase crystallization, a critical part of membrane protein crystallography, have also been developed allowing datasets to be collected from membrane proteins without the need for harvesting from the drop [75]. The wells of CrystalDirect plates [28] are designed to be laser cut and mounted on special pins to avoid crystal fishing, sidestepping some of the problems associated with *in situ* crystallography.

3.4. Complementary spectroscopic techniques

Several beamlines offer the acquisition of optical spectroscopic data concurrent with the collection of diffraction data sets [22,30,39,50,111,113,118,125,126,136]. Key applications of this complementary information are the identification of kinetic reaction intermediates in structural enzymology, as well as the quantitative monitoring of changing oxidation states of metal centers due to X-ray induced photoelectrons. The spectroscopic methods of choice are UV/Vis absorption, fluorescence, and Raman spectroscopy. The design of the micro-spectrophotometers differs considerably between the different beamlines. The range of methods offered varies from absorption spectroscopy, to combined absorption and fluorescence spectrometers, to the combination of all three methods listed above. While some implementations require a reconfiguration of the endstation, and therefore are typically operated in dedicated spectroscopy shifts, others are permanent installations. A further defining characteristic is the alignment of the optical axes with respect to the X-ray beam – on-axis systems provide an immediate view of the relative beam overlap, while off-axis systems require rotational realignments between diffraction and spectroscopic measurements. Since the acquisition of spectroscopic data can be considerably more time consuming than the diffraction experiment, several beamlines provide accompanying off-line laboratories to perform a spectroscopic pre-characterization of the crystals before taking them to the beamline.

3.5. Sample visualisation

High quality visualisation of samples is essential for accurate alignment of crystals in the X-ray beam. In its most simple implementation this takes the form of a standard microscope pointing at the sample position, though as beam and crystal sizes have reduced this approach has proved insufficient to accurately and reliably align crystals in the X-ray beam. On-axis video microscopes (OAV), such as that developed for the MD2 diffractometer [114], with a drilled objective and 45° mirror provide a view of the sample as seen from the source, and this arrangement is now considered standard at MX beamlines. OAV images and recognition algorithms are used to identify loops and automatically centre these in the X-ray beam [82,86,119]. It can be challenging, however, to apply such routines based on an optical microscope to small crystals or to crystals whose mother liquor becomes opaque in the cryo-cooling process. Errors of only a few microns are sufficient to move the crystal out of the X-ray beam during data collection.

In order to address some of these challenges, the optical properties of protein crystals can also be exploited to facilitate crystal identification and alignment. UV-induced fluorescence can be used to identify crystals [24,63,142] aiding automated alignment of crystals within loops. UV light provided by a laser or LED induces fluorescence from aromatic amino acids between 300 and 450 nm, which is readily detected by a standard microscope giving high contrast between crystals and the surrounding mother liquor. Second-order nonlinear optical imaging of chiral crystals (SONICC) has also recently been explored for imaging protein crystals [29,43,83]. This allows identification of protein crystals within opaque amorphous material such as lipidic cubic phase (LCP).

Where optical recognition is not possible, and for very small crystals, grid scanning can be used. The diffraction grid scan rasters samples through the X-ray beam resulting in a 2D map of diffraction images [1,17,25,135]. Automatic scoring of each image allows rapid visualisation of crystal location, or in the case of crystals larger than the beamsize, variations in diffracting power across a crystal. Sequential collection of grids at multiple angles is sufficient to ensure centering of a sample so it remains in the X-ray beam during data collection. Grid scanning is particularly applicable to crystals grown or cryocooled in opaque material. In the case of extremely small crystals, from which it is not possible to collect a large wedge of diffraction data, sequential grids often take the form of a coarse grid to locate crystals followed by a closely spaced grid to fine-tune the crystal position for data collection.

X-ray imaging, or tomography, can also be used to identify and characterise crystals [19,146]. The contrast in X-ray beam properties required for imaging means this approach has not become widely implemented, but it may prove of particular use at long wavelength beamlines where increased absorption of X-rays should be taken into account for optimal data processing.

3.6. Detectors

Macromolecular crystallography has benefited greatly from the development of large area detectors. In the early days of crystallography these took the form of X-ray sensitive film (1980s) and image plates (mid-1990s) before the introduction of CCD detectors to synchrotron sources (late 1990s). The increasing area of detectors allows data to be collected with improved signal to noise as the detector can be positioned further away from the sample when collecting data to a given resolution, especially when the beam is focused after the sample. This reduces the contribution of diffuse X-ray scatter to the recorded pattern, and increases the inter-spot separation. This and other aspects of optimal data collection are discussed by Ref. [37].

Until recently, the vast majority of MX beamlines were equipped with a CCD detector possessing a readout time on the order of a few seconds. At synchrotron sources this permitted a frame rate of one image every 2–3 s, with the X-ray shutter closing while the detector was read-out. During this time the goniometer would be stopped, wound back and then set rotating again ready for the next image in the dataset adding a time overhead and stringent requirements on synchronisation of beamline hardware. The advent of Pixel Array Detectors (PADs) for MX has revolutionised how data

are collected, with an increasing number of MX beamlines now equipped with a PAD.

A major advantage of PADs and the newest generation of CCD detectors over 'classical' detectors is their short readout time. Readout times of less than a millisecond can be achieved as all pixels on the detector are read-out in parallel. Pioneered for MX at the Swiss Light Source [47], and commercialised by Dectris, this allows 'continuous' data collection, where the crystal is continually rotated and the X-ray shutter remains open during data collection. This approach greatly simplifies shuttering and synchronisation of beamline hardware, and dramatically reduces the duration of the experiment.

The large increase in achievable frame-rate and absence of readout noise means that experimental protocols such as fine-phi slicing, which improve data quality [101,115], but would previously have been prohibitively time consuming are now considered routine.

The dramatic reduction in the data collection times that can be achieved from both advances in detector technology and beamline hardware has proven a driving force for automated sample exchange. The combination of these two developments means it can be considered routine to collect many hundreds of datasets in a single visit to a beamline.

The second type of detector present at all beamlines that support anomalous data collection is an energy dispersive X-ray Fluorescence (XRF) detector. By monitoring the element specific fluorescence line of a heavy atom scatterer while scanning the monochromator across its absorption edge, the exact position of the peak and inflection points of the edge can be determined using a program like CHOOCH [52], to optimize the anomalous signal. The most common form of detector in use is a silicon drift detector [137] which permits input count rates of up to 10^6 photons/s. To avoid detector saturation the beam intensity must therefore be carefully optimized to keep the detector dead time below values around 10–15%.

3.7. Sample delivery

Automated sample exchange has greatly benefited synchrotron MX allowing the high throughput promised by shorter exposure times and fast detector readout to be achieved. Increased throughput allows large numbers of crystals to be screened during a single visit which can prove to be essential when only a small fraction of crystals diffract well, and (or) when crystals are unsuitable for a home source. Automated sample exchange also permits remote access, which can facilitate large numbers of research groups accessing a beamline for short visits in a short period and regular access to facilities remote from the home laboratory.

Industrial multi-axis robots have been often used for sample mounting (for a list of systems, see references in Refs. [95,116] This approach has been sidestepped at some sources in favor of automounters with a limited range of movement (most notably the SC3 at the ESRF and the Berkeley automounter [134]). The strict requirements imposed by automated sample exchangers have driven the development of standardised sample mounts. The Structural Proteomics In Europe (SPINE) project developed a standard sample holder for general use [27] based on the Hampton CrystalCap, and the SPINE pin remains the standard at the majority of synchrotrons. Standardised containers for the transport of SPINE pins between sites, and mounting in sample changers have also been developed, with multiple standards (for example the Unipuck and ESRF/EMBL basket) co-existing. However, the increasing rate of crystal testing and collection is driving the development of even more compact pin designs such as the miniSpine and the NewPin standard,[4] that are currently being introduced.

The strict requirements on sample holder uniformity, the need to synchronise robots with other beamline equipment, and the necessary combination of moving components and liquid nitrogen has, coupled with the high success rates required for successful, ice-free, sample exchange, resulted in automation being a challenging area since the first auto-mounters were developed in the early 2000s [31,99].

To date, the majority of data collections at synchrotrons are carried out on single crystals individually mounted by hand on a holder. While in some cases, the number of crystals may be increased to double-digits, for example in the case of polyhedral crystals mounted on micromeshes [6], the number of crystals per mount nonetheless remains low. Experiments at Free Electron Lasers (FELs) have driven new modes of sample delivery, driven by the impact a single FEL pulse has on a protein crystal: with $> 10^{12}$ photons in a pulse of 5–50 fs, only a single still image can be collected before the sample is destroyed. Thousands of crystals are needed, driving the need for new modes of sample delivery.

A number of approaches have been developed to enable serial crystallography [23]. The most widely used has been the liquid jet or gas dynamic virtual nozzle [41] which streams a narrow jet of liquid containing crystals through the X-ray beam. High Viscosity Extrusion jets (or "toothpaste jets") with their slower flow speeds have since also been used at synchrotron beamlines [16,108]. Approaches more akin to those used at synchrotron sources have been developed as well. These are generally based on a goniometer 'borrowed' from a synchrotron beamline [32,72] and successes with this approach have led to the emergence of serial crystallography at synchrotrons [16,33,62]. On-going work in new sample mounts, such as grid-based supports [9,75,100,104,123] and microfluidic flow cells [44,70,89], may see sample delivery techniques optimal for use at both FELs and synchrotrons.

3.8. Sample lifetime

The loop mounting and cryo-cooling of protein crystals prior to data collection has had a dramatic effect on MX. Once cryo-cooled, crystals effectively become immortal (prior to exposure to X-rays), and sample transport and automatic mounting is greatly simplified. The development of techniques to optimize the cryo-cooling process [61] means that in a large fraction of cases, crystal quality is not adversely affected upon cooling to 100 K, though notable exceptions to this exist, for example in the field of virus crystallography. Cryo-cooling also provides a large benefit in terms of radiation damage, increasing the lifetime of crystals by a factor of ~70 [60].

Even the protection conferred by cryo-cooling does not allow radiation damage to be ignored however, and the finite lifetime of crystals is now frequently the primary reason for choosing the start angle for data collection with care. Site-specific damage means that in addition to a global decay in diffracting power during data collection the relative intensities of reflections change [35,112]. The magnitude of changes to individual reflections resulting from site-specific damage is comparable to the changes induced by the introduction of heavy atoms so the best possible anomalous data are collected with Friedel pairs recorded close together in time (dose). An elegant way of achieving this is through the use of a multi-axis goniometer.

In recent years there has been a resurgence in room temperature (RT) crystallography at synchrotron sources with facilities for *in situ* data collection developed at a number of sources [7,13,78]. Data collection from crystals held in a crystallization tray means the potentially damaging steps of crystal harvesting and the cryo-

[4] https://embl.fr/newpin/.

cooling process can be sidestepped. In some cases, most frequently in virus crystallography, successful cryo-cooling can prove impossible, meaning RT data collection is the only option for structure solution. In such cases *in situ* data collection eliminates the need to transfer crystals to capillaries. Even while cryo-cooling appears to be successful: the cooling process can introduce artefacts in side-chain interactions [79] or hide conformation diversity [55] making a RT structure highly desirable. Although the rapid onset of radiation damage means that it may be possible to collect only a few degrees of data from each crystal, strategies have been developed to exploit new instrumentation such as fast PADs and maximize the amount of data that can be collected from each crystal [109,110]. Approaches for identifying the similarity of different crystals and how to optimally merge data from these have also been developed [54,88]. The concomitant development of hardware and software optimised for RT data collection and processing means the approach can be applied to structure solution and phasing of challenging targets such as membrane proteins [5,75].

3.9. Data acquisition and processing

Key to the wide uptake of MX at synchrotron sources has been the development of control software to allow non-expert users carry out crystallography experiments. Control of the experiment usually relies on a high-level graphical software layer on top of the low-level beamline control system such as EPICS [36], TANGO [64] or MADOCA [93]. Some widely implemented systems are Blu-Ice [94], MxCuBE [59], GDA[5] and BSS [139]. To ensure the portability to different synchrotrons, some systems such as MXCuBE are encompassing a further dissection between the graphical interface (common to all facilities) and the functionality logic (particular to each beamline). The software layer can embrace all aspects of the experiment from sample loading and sample alignment to data collection and analysis. A high-level software layer allows complex data collections to become routine. Examples of this include automated grid X-ray scans, helical data collection, automatic adjustment of kappa goniometry, and interweaved (inverse beam) data collections. A reliable, comprehensive software layer is required for automatic beamline operation for hours through sample queueing, as well as for remote operation of the beamline.

The speed of data collection and throughput has dramatically increased in recent years. This is illustrated by 2 MAD experiments made 15 years apart, both taking approximately a little less than 25 min [45,144]. In 1999, a total of 240 images, 3 s exposure per image, were taken on one crystal at three wavelengths. In 2014, ~43,000 frames, 0.02 s exposure per frame, were taken on four crystals at four wavelengths each. The larger *quantity* of collected data has increased the productivity of the beamlines, as shown by the progressive increment of the maximum annual PDB releases achieved by the beamlines. It also favours the variety of successful projects, as more collection strategies are available (e.g. fine phi-slicing, multi-crystal data clustering).

Increases in throughput and speed mean that control systems face much tighter requirements on synchronisation and must be able to cope with large volumes of data. The amount of data generated boosts the need for automated data processing. This ranges from preliminary analysis of raw images, to automated phasing and structure solution. Pipelines such as *ELVES* [74], *xia2* [150], autoPROC [143], EDNA [98] and *MeshAndCollect* [151] aim to perform the automatic steps of the data processing, as well as to provide quick feedback on data already collected to optimize the following collections.

[5] http://www.opengda.org/OpenGDA.html.

As an umbrella to the experiments performed at the beamlines, Laboratory Information Management Systems (LIMS) such as ISPyB [40] allow large volumes of both raw data and the results of auto-processing to be tracked and managed also from home laboratory. In the future LIMS will likely be coupled to user and safety office databases.

4. Conclusions

In recent years, significant progress has been made in all aspects of MX experiments, from photon sources in storage rings to the management of processed data. Taken together, these developments have transformed what might be considered a typical visit to a MX beamline. Data can be collected and structures determined from samples that may not even be visible in a microscope. Diffraction images may not be indicative of the success of the experiment. Decision-making is sometimes the main bottleneck for data collection. Synchrotron users are not even required at synchrotrons anymore. All steps in the chain from crystal to structure can rely on robust instrumentation and automated control. In short, even complex MX experiments can become automated measurements. Synchrotron facilities, rather than just providing photons and raw data, are nowadays offering a full “user experience” and ready-to-interpret data at the end of every beamtime. Yet, human control is always possible in all steps, and in challenging cases is still required for the success of the experiment.

Beyond the most “standard” projects, the MX field is also rapidly evolving and beamlines dedicated to specific methods, for example long wavelength, microfocus or *in situ* data collection, will lead to advances in several divergent areas. New data collection strategies are also appearing. A real, future breakthrough is to come with the advent of 4th generation sources, which will push for new instrumentation, sample handling and phasing methods. It is not only structural biology driving the advances in MX beamline instrumentation and control, but also these new developments offering opportunities that science will find the way to exploit. Conceivably, the synergy between instrumentation and science will lead to new insights into the structure and function of macromolecules in the years to come.

One of the authors (JJ) is indebted to Prof. Joan Bordas and Salvador Ferrer for previous fruitful discussions on optics, experiments and beamline management.

References

[1] J. Aishima, R.L. Owen, D. Axford, E. Shepherd, G. Winter, K. Levik, P. Gibbons, A. Ashton, G. Evans, Acta Cryst. D66 (2010) 1032–1035.
[2] R.W. Alkire, G. Rosenbaum, G. Evans, J. Synchrotron Radiat. 7 (2000) 61–68.
[3] J. Als-Nielsen, D. McMorrow, Elements of Modern X-ray Physics, John Wiley & Sons, 2011.
[4] W.W. Arndt, A.J. Wonacott (Eds.), The Rotation Method in Crystallography: Data Collection from Macromolecular Crystals, North-Holland Publishing Co, 1977.
[5] D. Axford, J. Foadi, N.-J. Hu, H.G. Choudhury, S. Iwata, K. Beis, G. Evans, Y. Alguel, Acta Crystallogr. Sect. D. 71 (2015) 1228–1237.
[6] D. Axford, X. Ji, D.I. Stuart, G. Sutton, Acta Crystallogr. Sect. D. 70 (2014) 1435–1441.
[7] D. Axford, R. Owen, J. Aishima, J. Foadi, M. AW, J. Robinson, J. Nettleship, R. Owens, I. Moraes, E. Fry, K. Harlos, A. Kotecha, J.M. Grimes, J. Ren, G. Sutton, T.S. Walter, D.I. Stuart, G. Evans, Acta Cryst. D68 (2012) 592–600.
[8] W.J. Bartels, J. Vac. Sci. Technol. B 1 (1983) 338–345.
[9] E.L. Baxter, L. Aguila, R. Alonso-Mori, C.O. Barnes, C.A. Bonagura, W. Brehmer, A.T. Brunger, G. Calero, T.T. Caradoc-Davies, R. Chatterjee, W.F. Degrado, J.S. Fraser, M. Ibrahim, J. Kern, B.K. Kobilka, A.C. Kruse, K.M. Larsson, H.T. Lemke, A.Y. Lyubimov, A. Manglik, S.E. McPhillips, E. Norgren, S.S. Pang, S.M. Soltis, J. Song, J. Thomaston, Y. Tsai, W.I. Weis, R.A. Woldeyes, V. Yachandra, J. Yano, A. Zouni, A.E. Cohen, Acta Crystallogr. Sect. D. 72 (2016) 2–11.
[10] M. Bei, M. Borland, Y. Cai, P. Elleaume, R. Gerig, K. Harkay, L. Emery, A. Hutton, R. Hettel, R. Nagaoka, D. Robin, C. Steier, Nucl. Instrum. Methods Phys. Res. Sect. A Accel. Spectrom. Detect. Assoc. Equip. 622 (2010) 518–535.

[11] H.D. Bellamy, R.P. Phizackerley, S.M. Soltis, H. Hope, J. Appl. Crystallogr. 27 (1994) 967–970.
[12] D.H. Bilderback, A.K. Freund, G.S. Knapp, D.M. Mills, J. Synchrotron Radiat. 7 (2000) 53–60.
[13] R. Bingel-Erlenmeyer, V. Olieric, J.P.A. Grimshaw, J. Gabadinho, X. Wang, S.G. Ebner, A. Isenegger, R. Schneider, J. Schneider, W. Glettig, C. Pradervand, E.H. Panepucci, T. Tomizaki, M. Wang, C. Schulze-Briese, Cryst. Growth Des. 11 (2011) 916–923.
[14] C. Bloomer, J. Brandao-Neto, G. Rehm, C. Thomas, The Proceedings of the 9th European Workshop on Beam Diagnostics and Instrumentation for Particle Accelerators (DIPAC09), May, 2009, pp. 25–27.
[15] C. Bloomer, A. Dent, S. Diaz-Moreno, I. Dolbnya, U. Pedersen, G. Rehm, C. Tang, C. Thomas, J. Phys. Conf. Ser. 425 (2013) 042010.
[16] S. Botha, K. Nass, T.R.M. Barends, W. Kabsch, B. Latz, F. Dworkowski, L. Foucar, E. Panepucci, M. Wang, R.L. Shoeman, I. Schlichting, R.B. Doak, Acta Crystallogr. Sect. D. 71 (2015) 387–397.
[17] M.W. Bowler, M. Guijarro, S. Petitdemange, I. Baker, O. Svensson, M. Burghammer, C. Mueller-Dieckmann, E.J. Gordon, D. Flot, S.M. McSweeney, G.A. Leonard, Acta Cryst. D66 (2010) 855–864.
[18] M.W. Bowler, U. Mueller, M.S. Weiss, J. Sanchez-Weatherby, T.L.M. Sorensen, M.M.G.M. Thunnissen, T. Ursby, A. Gobbo, S. Russi, M.G. Bowler, S. Brockhauser, O. Svensson, F. Cipriani, Cryst. Growth & Des. 15 (2015) 1043–1054.
[19] S. Brockhauser, M. Di Michiel, J.E. McGeehan, A.A. McCarthy, R.B.G. Ravelli, J. Appl. Crystallogr. 41 (2008) 1057–1066.
[20] S. Brockhauser, R.B.G. Ravelli, A.A. McCarthy, Acta Crystallogr. Sect. D. 69 (2013) 1241–1251.
[21] J.C. Brooks-Bartlett, E.F. Garman, Interdiscip. Sci. Rev. 40 (2015) 244–264.
[22] P. Carpentier, A. Royant, J. Ohana, D. Bourgeois, J. Appl. Cryst. 40 (2007) 1113–1122.
[23] L.M.G. Chavas, L. Gumprecht, H.N. Chapman, Struct. Dyn. 2 (2015) 041709.
[24] L.M.G. Chavas, Y. Yamada, M. Hiraki, N. Igarashi, N. Matsugaki, S. Wakatsuki, J. Synchrotron Radiat. 18 (2011) 11–15.
[25] V. Cherezov, M.A. Hanson, M.T. Griffith, M.C. Hilgart, R. Sanishvili, V. Nagarajan, S. Stepanov, R.F. Fischetti, P. Kuhn, R.C. Stevens, J. R. Soc. Interface 6 (2009) S587–S597.
[26] J. Chrin, T. Schmidt, A. Streun, D. Zimoch, Nucl. Instrum. Methods Phys. Res. Sect. A Accel. Spectrom. Detect. Assoc. Equip. 592 (2008) 141–153.
[27] F. Cipriani, F. Felisaz, L. Launer, J.-S. Aksoy, H. Caserotto, S. Cusack, M. Dallery, F. di-Chiaro, M. Guijarro, J. Huet, S. Larsen, M. Lentini, J. McCarthy, S. McSweeney, R. Ravelli, M. Renier, C. Taffut, A. Thompson, G.A. Leonard, M.A. Walsh, Acta Crystallogr. Sect. D. 62 (2006) 1251–1259.
[28] F. Cipriani, M. Rower, C. Landret, U. Zander, F. Felisaz, J.A. Marquez, Acta Crystallogr. Sect. D. 68 (2012) 1393–1399.
[29] R.G. Closser, E.J. Gualtieri, J.A. Newman, G.J. Simpson, J. Appl. Crystallogr. 46 (2013) 1903–1906.
[30] A.E. Cohen, T. Doukov, S. Michael Soltis, Protein Pept. Lett. 23 (3) (2016) 283–290.
[31] A.E. Cohen, P.J. Ellis, M.D. Miller, A.M. Deacon, R.P. Phizackerley, J. Appl. Crystallogr. 35 (2002) 720–726.
[32] A.E. Cohen, S.M. Soltis, A. Gonzalez, L. Aguila, R. Alonso-Mori, C.O. Barnes, E.L. Baxter, W. Brehmer, A.S. Brewster, A.T. Brunger, G. Calero, J.F. Chang, M. Chollet, P. Ehrensberger, T.L. Eriksson, Y.P. Feng, J. Hattne, B. Hedman, M. Hollenbeck, J.M. Holton, S. Keable, B.K. Kobilka, E.G. Kovaleva, A.C. Kruse, H.T. Lemke, G.W. Lin, A.Y. Lyubimov, A. Manglik, Mathews II, S.E. McPhillips, S. Nelson, J.W. Peters, N.K. Sauter, C.A. Smith, J.H. Song, H.P. Stevenson, Y.S. Tsai, M. Uervirojnangkoorn, V. Vinetsky, S. Wakatsuki, W.I. Weis, O.A. Zadvornyy, O.B. Zeldin, D.L. Zhu, K.O. Hodgson, Proc. Natl. Acad. Sci. U. S. A. 111 (2014) 17122–17127.
[33] N. Coquelle, A.S. Brewster, U. Kapp, A. Shilova, B. Weinhausen, M. Burghammer, J.-P. Colletier, Acta Crystallogr. Sect. D. 71 (2015) 1184–1196.
[34] J.A. Cowan, C. Nave, J. Synchrotron Radiat. 15 (2008) 458–462.
[35] F. Crick, B. Magdoff, Acta Cryst. 9 (1956) 901–908.
[36] L.R. Dalesio, J.O. Hill, M. Kraimer, S. Lewis, D. Murray, S. Hunt, W. Watson, M. Clausen, J. Dalesio, Nucl. Instrum. Methods A 352 (1994) 179–184.
[37] Z. Dauter, Acta Crystallogr. Sect. D. 66 (2010) 389–392.
[38] Z. Dauter, M. Jaskolski, A. Wlodawer, J. Synchrotron Radiat. 17 (2010) 433–444.
[39] R.J. Davies, M. Burghammer, C. Riekel, J. Synchrotron. Rad. 16 (2009) 22–29.
[40] S. Delagenière, P. Brenchereau, L. Launer, A.W. Ashton, R. Leal, S. Veyrier, J. Gabadinho, E.J. Gordon, S.D. Jones, K.E. Levik, S.M. McSweeney, S. Monaco, M. Nanao, D. Spruce, O. Svensson, M.A. Walsh, G.A. Leonard, Bioinformatics 27 (2011) 3186–3192.
[41] D.P. DePonte, R.B. Doak, M. Hunter, Z. Liu, U. Weierstall, J.C.H. Spence, Micron 40 (2009) 507–509.
[42] K. Desjardins, M. Pomorski, J. Morse, J. Synchrotron Radiat. 21 (2014) 1217–1223.
[43] E.L. DeWalt, V.J. Begue, J.A. Ronau, S.Z. Sullivan, C. Das, G.J. Simpson, Acta Crystallogr. Sect. D. 69 (2013) 74–81.
[44] K. Dhouib, C. Khan Malek, W. Pfleging, B. Gauthier-Manuel, R. Duffait, G. Thuillier, R. Ferrigno, L. Jacquamet, J. Ohana, J.-L. Ferrer, A. Theobald-Dietrich, R. Giege, B. Lorber, C. Sauter, Lab Chip 9 (2009) 1412–1421.
[45] H. Dong, Q. Xiang, Y. Gu, Z. Wang, N.G. Paterson, P.J. Stansfeld, C. He, Y. Zhang, W. Wang, C. Dong, Nature 511 (2014) 52–56.
[46] E.M.H. Duke, L.N. Johnson, Proc. R. Soc. Lond. A Math. Phys. Eng. Sci. 466 (2010) 3421–3452.
[47] E.F. Eikenberry, C. Brönnimann, G. Hülsen, H. Toyokawa, R. Horisberger, B. Schmitt, C. Schulze-Briese, T. Tomizaki, Nucl. Instrum. Methods A 501 (2003) 260–266.
[48] D. Einfeld, Synchrotron Radiat. News 27 (2014) 4–7.
[49] D. Einfeld, M. Plesko, Nucl. Instrum. Methods Phys. Res. Sect. A Accel. Spectrom. Detect. Assoc. Equip. 335 (1993) 402–416.
[50] M.J. Ellis, S.G. Buffey, M.A. Hough, S.S. Hasnain, J. Synchrotron. Rad. 15 (2008) 433–439.
[51] G. Evans, D. Axford, R.L. Owen, Acta Cryst. D67 (2011) 261–270.
[52] G. Evans, R.F. Pettifer, J. Appl. Crystallogr. 34 (2001) 82–86.
[53] R.F. Fischetti, S. Xu, D.W. Yoder, M. Becker, V. Nagarajan, R. Sanishvili, M.C. Hilgart, S. Stepanov, O. Makarov, J.L. Smith, J. Synchrotron Radiat. 16 (2009) 217–225.
[54] J. Foadi, P. Aller, Y. Alguel, A. Cameron, D. Axford, R.L. Owen, W. Armour, D.G. Waterman, S. Iwata, G. Evans, Acta Cryst. D69 (2013) 1617–1632.
[55] J.S. Fraser, H. van den Bedem, A.J. Samelson, P.T. Lang, J.M. Holton, N. Echols, T. Alber, Proc. Natl. Acad. Sci. U. S. A. 108 (2011) 16247–16252.
[56] M.R. Fuchs, C. Pradervand, V. Thominet, R. Schneider, E. Panepucci, M. Grunder, J. Gabadinho, F.S.N. Dworkowski, T. Tomizaki, J. Schneider, A. Mayer, A. Curtin, V. Olieric, U. Frommherz, G. Kotrle, J. Welte, X. Wang, S. Maag, C. Schulze-Briese, M. Wang, J. Synchrotron Radiat. 21 (2014a) 340–351.
[57] M.R. Fuchs, R.M. Sweet, L.E. Berman, W.A. Hendrickson, O. Chubar, N. Canestrari, M. Idir, L. Yang, D.K. Schneider, J. Phys. Conf. Ser. 493 (2014b) 012021.
[58] J.D. Fuerst, C. Doose, Q. Hasse, Y. Ivanyushenkov, M. Kasa, Y. Shiroyanagi, AIP Conf. Proc. 1573 (2014) 1527–1534.
[59] J. Gabadinho, A. Beteva, M. Guijarro, V. Rey-Bakaikoa, D. Spruce, M.W. Bowler, S. Brockhauser, D. Flot, E.J. Gordon, D.R. Hall, B. Lavault, A.A. McCarthy, J. McCarthy, E. Mitchell, S. Monaco, C. Mueller-Dieckmann, D. Nurizzo, R.B.G. Ravelli, X. Thibault, M.A. Walsh, G.A. Leonard, S.M. McSweeney, J. Synchrotron Radiat. 17 (2010) 700–707.
[60] E. Garman, Acta Cryst. D66 (2010) 339–351.
[61] E. Garman, R.L. Owen, Methods in Molecular Biology, in: Macromolecular Crystallography Protocols, vol. 364, Humana Press, 2007, pp. 1–18.
[62] C. Gati, G. Bourenkov, M. Klinge, D. Rehders, F. Stellato, D. Oberthur, O. Yefanov, B.P. Sommer, S. Mogk, M. Duszenko, C. Betzel, T.R. Schneider, H.N. Chapman, L. Redecke, IUCrJ 1 (2014) 87–94.
[63] K.J. Gofron, N.E.C. Duke, Nucl. Instrum. Methods Phys. Res. Sect. A Accel. Spectrom. Detect. Assoc. Equip. 649 (2011) 216–218.
[64] A. Götz, E. Taurel, J. Pons, P. Verdier, J. Chaize, J. Meyer, F. Poncet, G. Heunen, E. Götz, A. Buteau, in: ICALEPCS2003, Gyeongju, October, 2003.
[65] V. Grama, D. Axford, G. Duller, M. Burt, R.L. Owen, MEDSI 2014,2014.
[66] T. Hara, T. Tanaka, H. Kitamura, T. Bizen, X. Maréchal, T. Seike, T. Kohda, Y. Matsuura, Phys. Rev. Special Top. – Accel. Beams 7 (2004) 050702.
[67] A. Harmsen, R. Leberman, G.E. Schulz, J. Mol. Biol. 104 (1976) 311–314.
[68] J. Hausmann, E. Christodoulou, M. Kasiem, V. De Marco, L.A. van Meeteren, W.H. Moolenaar, D. Axford, R.L. Owen, G. Evans, A. Perrakis, Acta Crystallogr. Sect. F. 66 (2010) 1130–1135.
[69] R. Hettel, J. Synchrotron Radiat. 21 (2014) 843–855.
[70] M. Heymann, A. Opthalage, J.L. Wierman, S. Akella, D.M.E. Szebenyi, S.M. Gruner, S. Fraden, IUCrJ 1 (2014) 349–360.
[71] K. Hirata, Y. Kawano, G. Ueno, K. Hashimoto, H. Murakami, K. Hasegawa, T. Hikima, T. Kumasaka, M. Yamamoto, J. Phys. Conf. Ser. 425 (2013) 012002.
[72] K. Hirata, K. Shinzawa-Itoh, N. Yano, S. Takemura, K. Kato, M. Hatanaka, K. Muramoto, T. Kawahara, T. Tsukihara, E. Yamashita, K. Tono, G. Ueno, T. Hikima, H. Murakami, Y. Inubushi, M. Yabashi, T. Ishikawa, M. Yamamoto, T. Ogura, H. Sugimoto, J.-R. Shen, S. Yoshikawa, H. Ago, Nat. Methods 11 (2014) 734–736.
[73] K. Holldack, D. Ponwitz, W.B. Peatman, Nucl. Instrum. Methods Phys. Res. Sect. A Accel. Spectrom. Detect. Assoc. Equip. 467–468 (2001) 213–220. Part 1.
[74] J. Holton, T. Alber, Proc. Natl. Acad. Sci. U. S. A. 101 (2004) 1537–1542.
[75] C.-Y. Huang, V. Olieric, P. Ma, E. Panepucci, K. Diederichs, M. Wang, M. Caffrey, Acta Crystallogr. Sect. D. 71 (2015) 1238–1256.
[76] P. Ilinski, J. Phys. Conf. Ser. 425 (2013) 042006.
[77] L. Jacquamet, J. Ohana, J. Joly, F. Borel, M. Pirocchi, P. Charrault, A. Bertoni, P. Israel-Gouy, P. Carpentier, F. Kozielski, D. Blot, J.L. Ferrer, Structure 12 (2004a) 1219–1225.
[78] L. Jacquamet, J. Ohana, J. Joly, P. Legrand, R. Kahn, F. Borel, M. Pirocchi, P. Charrault, P. Carpentier, J.L. Ferrer, Acta Cryst. D60 (2004b) 888–894.
[79] D. Juers, B. Matthews, Acta Cryst. D60 (2004) 412–421.
[80] J. Juanhuix, F. Gil-Ortiz, G. Cuni, C. Colldelram, J. Nicolás, J. Lidón, E. Boter, C. Ruget, S. Ferrer, J. Benach, J. Synchrotron. Rad. 21 (2014) 679–689.
[81] A. Kachatkou, N. Kyele, P. Scott, R. van Silfhout, J. Synchrotron Radiat. 20 (2013) 596–602.
[82] W.I. Karain, G.P. Bourenkov, H. Blume, H.D. Bartunik, Acta Cryst. Crystallogr. Sect. D. 58 (2002) 1519–1522.
[83] D.J. Kissick, E.J. Gualtieri, G.J. Simpson, V. Cherezov, Anal. Chem. 82 (2010) 491–497.
[84] B. Knapp, E. Marsh, F. Cipriani, D. Arneson, D. Oss, M. Liebers, E. Keller, J. Phys. Conf. Ser. 425 (2013) 012012.
[85] A. Krolzig, G. Materlik, M. Swars, J. Zegenhagen, Nucl. Instrum. Methods Phys.

Res. 219 (1984) 430–434.
[86] B. Lavault, R.B.G. Ravelli, F. Cipriani, Acta Crystallogr. Sect. D. 62 (2006) 1348–1357.
[87] A. le Maire, M. Gelin, S. Pochet, F. Hoh, M. Pirocchi, J.-F. Guichou, J.-L. Ferrer, G. Labesse, Acta Crystallogr. Sect. D. 67 (2011) 747–755.
[88] Q. Liu, T. Dahmane, Z. Zhang, Z. Assur, J. Brasch, L. Shapiro, F. Mancia, W.A. Hendrickson, Science 336 (2012) 1033–1037.
[89] A.Y. Lyubimov, T.D. Murray, A. Koehl, I.E. Araci, M. Uervirojnangkoorn, O.B. Zeldin, A.E. Cohen, S.M. Soltis, E.L. Baxter, A.S. Brewster, N.K. Sauter, A.T. Brunger, J.M. Berger, Acta Crystallogr. Sect. D. 71 (2015) 928–940.
[90] A.A. MacDowell, R.S. Celestre, M. Howells, W. McKinney, J. Krupnick, D. Cambie, E.E. Domning, R.M. Duarte, N. Kelez, D.W. Plate, C.W. Cork, T.N. Earnest, J. Dickert, G. Meigs, C. Ralston, J.M. Holton, T. Alber, J.M. Berger, D.A. Agard, H.A. Padmore, J. Synchrotron Radiat. 11 (2004) 447–455.
[91] J.T. Madden, S.J. Toth, C.M. Dettmar, J.A. Newman, R.A. Oglesbee, H.G. Hedderich, R.M. Everly, M. Becker, J.A. Ronau, S.K. Buchanan, V. Cherezov, M.E. Morrow, S. Xu, D. Ferguson, O. Makarov, C. Das, R. Fischetti, G.J. Simpson, J. Synchrotron Radiat. 20 (2013) 531–540.
[92] M. Marinelli, E. Milani, G. Prestopino, C. Verona, G. Verona-Rinati, M. Angelone, M. Pillon, V. Kachkanov, N. Tartoni, M. Benetti, D. Cannata, F. Di Pietrantonio, J. Synchrotron Radiat. 19 (2012) 1015–1020.
[93] T. Matsumoto, Y. Furukawa, M. Ishii, Proceedings of ICALEPCS2013, San Francisco, USA, 2013, 944–947.
[94] T. Mcphillips, S. Mcphillips, H. Chiu, A. Cohen, A. Deacon, P. Ellis, E. Garman, A. Gonzalez, N. Sauter, R. Phizackerley, S. Soltis, P. Kuhn, J. Synchrotron. Rad. 9 (2002) 401–406.
[95] S. McSweeney, in: R. Read, A.G. Urzhumtsev, V.Y. Lunin (Eds.), NATO Science for Peace and Security Series a: Chemistry and Biology, Advancing Methods for Biomolecular Crystallography, Springer, Netherlands, 2013, pp. 47–57.
[96] A. Meents, B. Reime, N. Stuebe, P. Fischer, M. Warmer, D. Goeries, J. Roever, J. Meyer, J. Fischer, A. Burkhardt, I. Vartiainen, P. Karvinen, C. David, 2013, pp. 88510K-88510K-88517.
[97] R.H. Menk, D. Giuressi, F. Arfelli, L. Rigon, AIP Conf. Proc. (2006) 1109–1112.
[98] S. Monaco, E. Gordon, M.W. Bowler, S. Delageniere, M. Guijarro, D. Spruce, O. Svensson, S.M. McSweeney, A.A. McCarthy, G. Leonard, M.H. Nanao, J. Appl. Crystallogr. 46 (2013) 804–810.
[99] S. Muchmore, J. Olson, R. Jones, J. Pan, M. Blum, J. Greer, S. Merrick, P. Magdalinos, V. Nienaber, Structure 8 (2000) R243–r246.
[100] C. Mueller, A. Marx, S.W. Epp, Y. Zhong, A. Kuo, A.R. Balo, J. Soman, F. Schotte, H.T. Lemke, R.L. Owen, E.F. Pai, A.R. Pearson, J.S. Olson, P.A. Anfinrud, O.P. Ernst, R.J.D. Miller, Struct. Dyn. 2 (2015) 054302.
[101] M. Mueller, M. Wang, C. Schulze-Briese, Acta Cryst. D68 (2011) 42–56.
[102] C. Mueller-Dieckmann, M. Bowler, P. Carpentier, D. Flot, A. McCarthy, M. Nanao, D. Nurizzo, P. Pernot, A. Popov, A. Round, A. Royant, D. de Sanctis, D. von Stetten, G. Leonard, Eur. Phys. J. Plus 130 (2015) 1–11.
[103] E.M. Muller, J. Smedley, J. Bohon, X. Yang, M. Gaowei, J. Skinner, G. De Geronimo, M. Sullivan, M. Allaire, J.W. Keister, L. Berman, A. Heroux, J. Synchrotron Radiat. 19 (2012) 381–387.
[104] T.D. Murray, A.Y. Lyubimov, C.M. Ogata, H. Vo, M. Uervirojnangkoorn, A.T. Brunger, J.M. Berger, Acta Crystallogr. Sect. D. 71 (2015) 1987–1997.
[105] V. Mykhaylyk, A. Wagner, J. Phys. Conf. Ser. 425 (2013) 012010.
[106] N. Nakamura, T. Katsura, Particle Accelerator Conference, 1993., Proceedings of the 1993, 1993, vol. 2253, pp. 2257–2259.
[107] C. Nave, Acta Crystallogr. Sect. D. 55 (1999) 1663–1668.
[108] P. Nogly, D. James, D. Wang, T.A. White, N. Zatsepin, A. Shilova, G. Nelson, H. Liu, L. Johansson, M. Heymann, K. Jaeger, M. Metz, C. Wickstrand, W. Wu, P. Bath, P. Berntsen, D. Oberthuer, V. Panneels, V. Cherezov, H. Chapman, G. Schertler, R. Neutze, J. Spence, I. Moraes, M. Burghammer, J. Standfuss, U. Weierstall, IUCrJ 2 (2015) 168–176.
[109] R.L. Owen, D. Axford, J.E. Nettleship, R.J. Owens, J.I. Robinson, A.W. Morgan, A.S. Dore, G. Lebon, C.G. Tate, E.E. Fry, J. Ren, D.I. Stuart, G. Evans, Acta Cryst. D68 (2012) 810–818.
[110] R.L. Owen, N. Paterson, D. Axford, J. Aishima, C. Schulze-Briese, J. Ren, E.E. Fry, D.I. Stuart, G. Evans, Acta Crystallogr. Sect. D. 70 (2014) 1248–1256.
[111] R.L. Owen, A.R. Pearson, A. Meents, P. Boehler, V. Thominet, C. Schulze-Briese, J. Synchrotron. Rad. 16 (2009) 173–182.
[112] R.L. Owen, D.A. Sherrell, Acta Cryst. D72 (2016) 388–394. http://dx.doi.org/10.1107/S2059798315021555.
[113] A.R. Pearson, R. Pahl, E.G. Kovaleva, V.L. Davidson, C.M. Wilmot, J. Synchrotron. Rad. 14 (2007) 92–98.
[114] A. Perrakis, F. Cipriani, J.-C. Castagna, L. Claustre, M. Burghammer, C. Riekel, S. Cusack, Acta Cryst. D55 (1999) 1765–1770.
[115] J. Pflugrath, Acta Cryst. D55 (1999) 1718–1725.
[116] J. Pflugrath, Acta Crystallogr. Sect. F. 71 (2015) 622–642.
[117] J.C. Phillips, A. Wlodawer, M.M. Yevitz, K.O. Hodgson, Proc. Natl. Acad. Sci. 73 (1976) 128–132.
[118] G. Pompidor, F.S.N. Dworkowski, V. Thominet, C. Schulze-Briese, M.R. Fuchs, J. Synchrotron Radiat. 20 (2013) 765–776.
[119] S.B. Pothineni, T. Strutz, V.S. Lamzin, Acta Crystallogr. Sect. D. 62 (2006) 1358–1368.
[120] G. Rehm, J. Phys. Conf. Ser. 425 (2013) 042001.
[121] C. Riekel, M. Burghammer, G. Schertler, Curr. Opin. Struct. Biol. 15 (2005) 556–562.
[122] M. Robertson, Nature 285 (1980) 358–359.
[123] P. Roedig, I. Vartiainen, R. Duman, S. Panneerselvam, N. Stübe, O. Lorbeer, M. Warmer, G. Sutton, D.I. Stuart, E. Weckert, C. David, A. Wagner, A. Meents, Sci. Rep. 5 (2015).
[124] G. Rosenbaum, K. Holmes, J. Witz, Nature 230 (1971) 434–437.
[125] A. Royant, P. Carpentier, J. Ohana, J. McGeehan, B. Paetzold, M. Noirclerc-Savoye, X. Vernede, V. Adam, D. Bourgeois, J. Appl. Cryst. 40 (2007) 1105–1112.
[126] K. Sakai, Y. Matsui, T. Kouyama, Y. Shiro, S.-i. Adachi, J. Appl. Cryst. 35 (2002) 270–273.
[127] J. Sanchez-Weatherby, M.W. Bowler, J. Huet, A. Gobbo, F. Felisaz, B. Lavault, R. Moya, J. Kadlec, R.B.G. Ravelli, F. Cipriani, Acta Crystallogr. Sect. D. 65 (2009) 1237–1246.
[128] M. Sato, N. Shibata, Y. Morimoto, Y. Takayama, K. Ozawa, H. Akutsu, Y. Higuchi, N. Yasuoka, J. Synchrotron. Rad. 11 (2004) 113–116.
[129] W. Schildkamp, C. Pradervand, Rev. Sci. Instrum. 66 (1995) 1956–1959.
[130] H. Sehr, C. Schulze-Briese, C. Pradervand, H. Schift, J. Gobrecht, Technical Digest of Eurosensors XVIII, 2004, pp. 212–215.
[131] D. Shu, T.M. Kuzay, Y. Fang, J. Barraza, T. Cundiff, J. Synchrotron Radiat. 5 (1998) 636–638.
[132] O. Singh, G. Decker, 2001 Particle Accelerator Conference, PAC 2001. Proceedings of the 2001, 2001, vol. 531, pp. 539–543.
[133] J.L. Smith, R.F. Fischetti, M. Yamamoto, Curr. Opin. Struct. Biol. 22 (2012) 602–612.
[134] G. Snell, C. Cork, R. Nordmeyer, E. Cornell, G. Meigs, D. Yegian, J. Jaklevic, J. Jin, R. Stevens, T. Earnest, Structure 12 (2004) 537–545.
[135] J. Song, D. Mathew, S.A. Jacob, L. Corbett, P. Moorhead, S.M. Soltis, J. Synchrotron. Rad. 14 (2007) 191–195.
[136] D. Stoner-Ma, J.M. Skinner, D.K. Schneider, M. Cowan, R.M. Sweet, A.M. Orville, J. Synchrotron. Rad. 18 (2010) 37–40.
[137] L. Struder, C. Fiorini, E. Gatti, R. Hartmann, P. Holl, N. Krause, P. Lechner, A. Longoni, G. Lutz, J. Kemmer, N. Meidinger, M. Popp, H. Soltau, U. Weber, C. von Zanthier, J. Synchrotron Radiat. 5 (1998) 268–274.
[138] P.F. Tavares, S.C. Leemann, M. Sjostrom, A. Andersson, J. Synchrotron Radiat. 21 (2014) 862–877.
[139] G. Ueno, H. Kanda, T. Kumasaka, M. Yamamoto, J. Synchrotron Radiat. 12 (2005) 380–384.
[140] R. van Silfhout, A. Kachatkou, E. Groppo, C. Lamberti, W. Bras, J. Synchrotron Radiat. 21 (2014) 401–408.
[141] G.B.M. Vaughan, J.P. Wright, A. Bytchkov, M. Rossat, H. Gleyzolle, I. Snigireva, A. Snigirev, J. Synchrotron Radiat. 18 (2011) 125–133.
[142] X. Vernede, B. Lavault, J. Ohana, D. Nurizzo, J. Joly, L. Jacquamet, F. Felisaz, F. Cipriani, D. Bourgeois, Acta Crystallogr. Sect. D. 62 (2006) 253–261.
[143] C. Vonrhein, C. Flensburg, P. Keller, A. Sharff, O. Smart, W. Paciorek, T. Womack, G. Bricogne, Acta Crystallogr. Sect. D. 67 (2011) 293–302.
[144] M. Walsh, I. Dementieva, G. Evans, R. Sanishvili, A. Joachimiak, Acta Cryst. D55 (1999) 1168–1173.
[145] S. Waltersperger, V. Olieric, C. Pradervand, W. Glettig, M. Salathe, M.R. Fuchs, A. Curtin, X. Wang, S. Ebner, E. Panepucci, T. Weinert, C. Schulze-Briese, M. Wang, J. Synchrotron Radiat. 22 (2015) 895–900.
[146] A.J. Warren, W. Armour, D. Axford, M. Basham, T. Connolley, D.R. Hall, S. Horrell, K.E. McAuley, V. Mykhaylyk, A. Wagner, G. Evans, Acta Crystallogr. Sect. D. 69 (2013) 1252–1259.
[147] E. Weckert, IUCrJ 2 (2015) 230–245.
[148] T. Weitkamp, B. Nöhammer, A. Diaz, C. David, E. Ziegler, Appl. Phys. Lett. 86 (2005) 054101.
[149] F. Willeke, 2015, Brookhaven National Laboratory (BNL).
[150] G. Winter, J. Appl. Crystallogr. 43 (2010) 186–190.
[151] U. Zander, G. Bourenkov, A.N. Popov, D. de Sanctis, O. Svensson, A.A. McCarthy, E. Round, V. Gordeliy, C. Mueller-Dieckmann, G.A. Leonard, Acta Crystallogr. Sect. D. 71 (2015) 2328–2343.
[152] O.B. Zeldin, M. Gerstel, E.F. Garman, J. Appl. Crystallogr. 46 (2013) 1225–1230.
[153] T. Zhou, W. Ding, M. Gaowei, G. De Geronimo, J. Bohon, J. Smedley, E. Muller, J. Synchrotron Radiat. 22 (2015) 1396–1402.
[154] R. Signorato, O. Hignette, J. Goulon, J. Synchrotron Rad 5 (1998) 797–800.
[155] L. Peverini, I.V. Kozhevnikov, A. Rommeveaux, P.V. Vaerenbergh, L. Claustre, S. Guillet, J.-Y. Massonnat, E. Ziegler, J. Susini, Nucl. Instrum. Methods Phys. Res. A 616 (2010) 115–118.
[156] K. Yamauchi, H. Mimura, K. Inagaki, Y. Mori, Rev. Sci. Instrum 73 (2002) 4028.
[157] F. Siewert, J. Buchheim, T. Zeschke, M. Störmer, G. Falkenbergc, R. Sankari, On the characterization of ultra-precise X-ray optical components: advances and challenges in ex situ metrology, J. Synchrotron Rad 21 (2014) 968–975.
[158] A. Snigirev, V. Kohn, I. Snigireva, B. Lengeler, Nature 384 (07 November 1996) 49–51.
[159] M.W. Bowler, D. Nurizzo, R. Barrett, A. Beteva, M. Bodin, H. Caserotto, S. Delagenière, F. Dobias, D. Flot, T. Giraud, N. Guichard, M. Guijarro, M. Lentini, G.A. Leonard, S. McSweeney, M. Oskarsson, W. Schmidt, A. Snigirev, D. von Stetten, J. Surr, O. Svensson, P. Theveneau, C. Mueller-Dieckmann, J. Synchrotron Rad 22 (2015) 1540–1547. http://dx.doi.org/10.1107/S1600577515016604.